NATIONAL RADIO ASTRONOMY OBSERVATORY
Green Bank, West Virginia

Electronics Division Internal Report No. 40

NRAO INTERFEROMETER: DESIGN, OPERATION, AND EARLY RESULTS

Nigel J. Keen

NOVEMBER 1964

NUMBER OF COPIES: 75

NRAO INTERFEROMETER: DESIGN, OPERATION AND EARLY RESULTS

Nigel J. Keen

ABSTRACT

The NRAO interferometer is described, together with first calibration results and some early observational data. The delay tracking procedure permits more than ten consecutive hours of observation of one source, with the continuous output of data on the two-dimensional source brightness distributions; this delay tracking facility is also utilized in a radio baseline survey which yields results at least as accurate as the normal geodetic survey. With a baseline of approximately 11,000 λ, day-to-day rms phase fluctuations at interferometer equator transit range from 20° to 40°, depending on the time of day. Larger phase variations appear to occur away from the instrumental equator. The final section contains a summary of early results on the interferometer.

I. INTRODUCTION

The two 85-foot antennas at NRAO are operated as an interferometer with baseline azimuth 62°, with seven available baseline lengths along this azimuth, by moving the southwestern antenna. Signal and image bands are accepted, with the IF passband from 2 to 12 MHz. The local oscillator frequency is 2695 MHz.

Section II describes the information theoretically available from a tracking interferometer. Section III considers the correlation response and briefly compares the performance of total power and correlation receivers. Section IV describes the equipment. Section V deals with an important characteristic of the instrument: the point at which the fringe rate becomes zero. Section VI describes some equator and off-equator transit results, and the first results of continuous delay tracking. Section VII briefly considers future developments.

A simple introduction to radio interferometry is given in reference [1].

II. INFORMATION AVAILABLE FROM A DELAY TRACKING INTERFEROMETER

Read [2] and Rowson [3] have shown that an interferometer projects fringe maxima on the celestial sphere where

$$\frac{n\lambda}{D} = \sin \Theta$$

$$\text{i.e., } \frac{n\lambda}{D} = \sin d \sin \delta + \cos d \cos \delta \cos (H - h) \qquad (1)$$

where δ = declination of the considered point on the celestial sphere,

H = hour angle of the considered point on the celestial sphere,

d = declination of pole of the interferometer,

h = hour angle of pole of the interferometer,

Θ = zenith angle of interferometer (see Figure I),

λ = central operating wavelength ($\lambda = \lambda_{LO}$ for double passband system),

D = baseline (distance between antennas), and

n = an integer.

The pole of the baseline is the declination of the point of intersection of the baseline with the celestial sphere. For the moment we neglect such instrumental effects as bandwidth and phase jitter. Individual antennas track the source being observed.

The disposition of fringes upon the celestial sphere, according to equation (1), is shown in Figure II: the angles given are for the NRAO interferometer. F_0 corresponds to the zenith fringe, n = 0.

Away from the instrumental equator, the projected length and orientation of the baseline (on the source) changes with source declination and hour angle. Observing a source continuously gives considerable data on its brightness distribution. Arsac [4] has pointed out that the interferometer is a spatial frequency filter. Since spatial frequency distributions are the fourier transformations of brightness distributions, it is more reasonable to present interferometer data in the spatial frequency ("fringe visibility") plane, at least until this plane has been reasonably filled (out to the resolution required) with the amplitudes and phases of the spatial frequency components. The restoration of brightness distributions in this "aperture synthesis" technique has been considered by Bracewell [5] and by Ryle and Hewish [6]. The subject of restoration will not be treated here.

Rowson has shown that, when an interferometer tracks a source, data for a source of given declination follows an elliptical track in the spatial frequency plane. The tracks for the NRAO interferometer, for sources at various declinations, are shown in Figure III. These tracks are "smeared" by finite bandwidth and individual antenna diameters. For an interferometer with an East-West baseline, tracks would be symmetrical about the u-axis, and would cross the v-axis at an hour angle of 6 hours (East and West), where u and v are the cartesian coordinates of spatial frequency. For the NRAO interferometer one v-axis crossing is at an hour angle of approximately 4 hours 50 minutes West. This crossing is an important instrumental parameter, and will be considered further in Section IV.

It is often more convenient to use the circular coordinates F and ρ in describing points in the spatial frequency plane. F is the projected relative baseline length, so that F = 1 at meridian transit. The angle between the projection of the baseline on the source and celestial North-South is the angle ρ. A typical F and ρ are shown in Figure III. The equations for F and ρ are:

$$F = \cos \beta$$

$$\sin \beta = \cos \varphi \cos A \sin \delta - \sin \varphi \cos A \cos \delta \cos H - \sin A \cos \delta \sin H \quad (3)$$

$$\tan \rho = \frac{\sin A \cos H - \sin \varphi \cos A \sin H}{\cos \varphi \cos A \cos \delta + \sin \varphi \cos A \sin \delta \cos H + \sin A \sin \delta \sin H}$$

where A = baseline azimuth, and φ = geographic latitude.

Also, the spatial fringe period along the circular source track is

$$\frac{\lambda}{\text{D. F.}} \cdot \frac{1}{\cos \delta \sin \rho} \quad \text{radians}$$

$$= \frac{\lambda}{\text{D. F.}} \cdot \frac{24 \times 3600}{2\pi \cos \delta \sin \rho} \quad \text{sidereal seconds.}$$

Hence the fringe frequency is

$$\frac{\text{D. F.}}{\lambda} \cdot \frac{2\pi \cos \delta \sin \rho}{24 \times 3600} \quad \text{cycles per sidereal second} \quad (5)$$

The above equations have been derived by Wade [7].

Differentiating equation (1) with respect to time

$$\frac{dn}{dt} = -\frac{D}{\lambda} \cdot \frac{dH}{dt} \cdot \cos d \cos \delta \sin (H - h) \quad (6)$$

$$= \text{fringe frequency.}$$

Hence, from (5) and (6)

$$F \sin \rho = \cos d \sin (H - h). \quad (7)$$

III. THE CROSS CORRELATION OF SIGNALS FROM THE TWO ANTENNAS

The response of the NRAO interferometer is due to cross-correlating the signals from each antenna. The possibility of cross-correlating at radio frequencies has been considered, but there are two objections:

(a) a.RF correlator is difficult to realize in practice, and

(b) the advantages of IF delay switching (that the fringes remain fixed on the sky as the source is tracked) are lost.

Let us compare RF and IF correlation.

(i) RF correlation. -- Consider the correlation (multiplication and integration) of two white stationary noise voltages after each has passed through the RF passband shown in Figure IV.

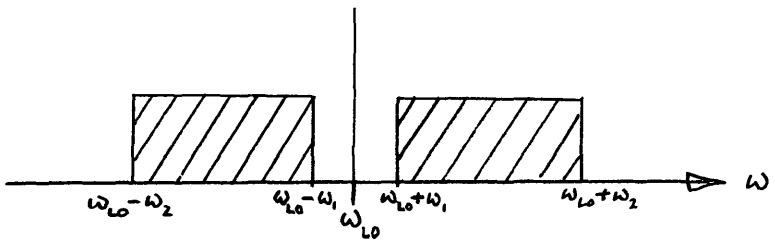

Figure IV

$F(\omega)$ = a constant where $\omega_{LO} - \omega_2 < \omega < \omega_{LO} - \omega_1$ and $\omega_{LO} + \omega_1 < \omega < \omega_{LO} + \omega_2$

= 0 outside these ranges.

Let the constant be unity.

If f(t) is the fourier transformation of the passband $F(\omega)$, the cross-correlation gives

$$R(\tau) = \int_{-\infty}^{\infty} f(t) \cdot f(\tau - t)\, dt$$

= correlator output response.

In Appendix I it is shown that $R(\tau)$ is the fourier transformation of the power response $G(\omega)$ at one antenna. Hence

$$G(\omega) = \left|F(\omega)\right|^2$$

$$R(\tau) = \int_{\omega_{LO} - \omega_2}^{\omega_{LO} - \omega_1} \cos \omega\tau \, d\omega + \int_{\omega_{LO} + \omega_1}^{\omega_{LO} + \omega_2} \cos \omega\tau \, d\omega$$

$$= \frac{1}{\tau} \left[\sin (\omega_{LO} - \omega_1)\tau - \sin (\omega_{LO} - \omega_2)\tau + \sin (\omega_{LO} + \omega_2)\tau - \sin (\omega_{\omega} + \omega_1)\tau\right]$$

$$= \frac{4}{\tau} \cdot \cos \omega_{LO}\tau \cdot \cos \frac{\left(\omega_2 + \omega_1\right)\tau}{2} \cdot \sin \frac{\left(\omega_2 - \omega_1\right)\tau}{2}$$

$$= 2\Delta\omega \cos \omega_{LO}\tau \cdot \cos \omega_{IF_0}\tau \cdot \frac{\sin \frac{\Delta\omega\tau}{2}}{\frac{\Delta\omega\tau}{2}}$$

The modulation of the RF fringes is given by the term

$$2\Delta\omega \cos \omega_{IF_0}\tau \, \frac{\sin \frac{\Delta\omega\tau}{2}}{\frac{\Delta\omega\tau}{2}} \tag{8}$$

Since $\cos \omega_{LO}\tau$ term represents the RF fringes, the position of the fringes on the sky will vary as the source is tracked (by varying τ).

(ii) IF correlation. -- We now consider the response of a correlation interferometer when the correlation occurs at IF — after superheterodyning the RF passband and IF filtering.

Monochromatic signals of angular frequency $(\omega_{LO} \pm \omega_1)$ arrive at the output of the mixer at each antenna (Fig. V), and may be represented, respectively, by

$$f_1(t) = [\cos \omega_{LO} t + \cos (\omega_{LO} + \omega_1)(t - T)]^2 + [\cos \omega_{LO} t + \cos (\omega_{LO} - \omega_1)(t - T)]^2$$

$$f_2(t) = [\cos \omega_{LO} t + \cos (\omega_{LO} + \omega_1) t]^2 + [\cos \omega_{LO} t + \cos (\omega_{LO} - \omega_1) t]^2$$

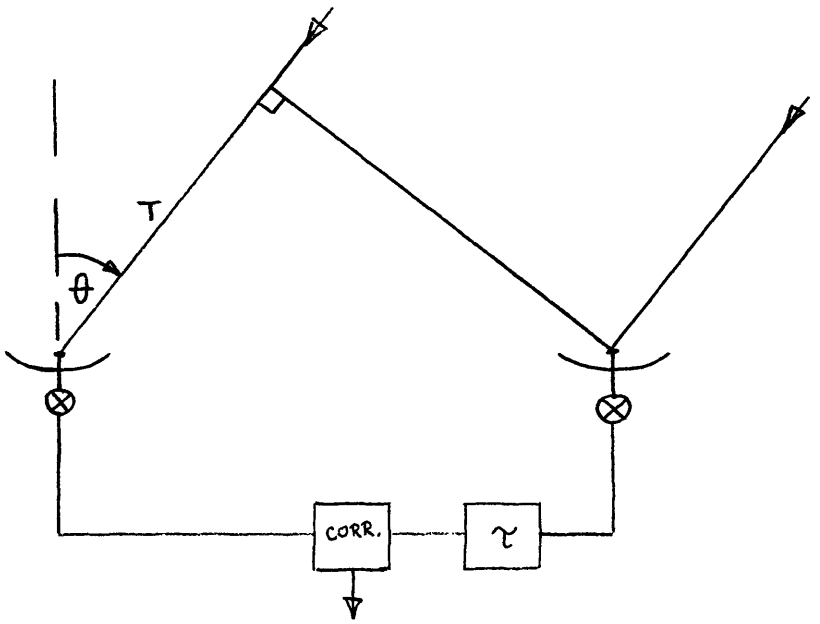

Figure V

Considering the delayed case (which is completely general), the part of $f_1(t)$ which would pass through the IF filter is

$$f(t) = 2 \cos \omega_{LO} t \, [\cos \omega_{LO} + \omega_1)(t - T) + \cos (\omega_{LO} - \omega_1)(t - T)]$$

This simplifies to

$$f(t) = 4 \, [\cos \omega_{LO} (2t - T) + \cos \omega_{LO} T] \cos \omega_1 (t - T)$$

Since the term in $\cos \omega_{LO} (2t - T)$ will be rejected by the IF filters, we now have

$$f(t) = 4 \cos \omega_{LO} T \cos \omega_1 (t - T).$$

For finite rectangular IF bandpasses,

$$f(t) = 4 \cos \omega_{LO} T \frac{\sin \Delta\omega(t - T)}{\Delta\omega(t - T)}$$

Hence, proceeding as before

$$R(\tau) = 16 \cos \omega_{LO} T \int_{-\infty}^{\infty} \frac{\sin \Delta\omega(t - T)}{\Delta\omega(t - T)} \cdot \frac{\sin \Delta w(t - T - \tau)}{\Delta\omega(t - T - \tau)} dt \qquad (9)$$

In practice the limits of integration in equation (9) are $-\phi$ and $+\phi$, where ϕ is the post-multiplication integration time. Hence

$$R(\tau) = 16 \cos \phi_{LO} T \int_{-\phi}^{+\phi} \frac{\sin \Delta\omega(t - T)}{\Delta\omega(t - T)} \cdot \frac{\sin \Delta\omega(t - T - \tau)}{\Delta\omega(t - T - \tau)} \qquad (10)$$

Also, the term outside the integral is actually of the form

$$\cos \omega_{LO}(T + \tau_{RF1}) \cos \omega_{LO} \tau_{RF2}$$

where differential phase variations in the local oscillator path are represented by a variation in $(\tau_{RF1} - \tau_{RF2})$. However, $\phi >> T$ and $(\tau_{RF1} - \tau_{RF2})$ is assumed constant, so that equation (9) represents the practical case. Proceeding as for RF correlation, we now have

$$R(\tau) = \frac{16}{T - \tau} \cdot \cos \omega_{LO} T \cos \frac{\omega_2 + \omega_1}{2} (T - \tau) \sin \frac{\omega_2 - \omega_1}{2} (T - \tau)$$

where T = the differential RF delay and τ = the differential IF delay. Hence the response is

$$\cos \omega_{LO} T \cdot \cos \omega_{IF} (T - \tau) \frac{\sin \frac{\Delta\omega(T - \tau)}{2}}{\frac{\Delta\omega(T - \tau)}{2}} \qquad (11)$$

which is similar to the case of direct RF correlation, with the important exception of the absence of τ in the term in ω_{LO}. Hence the RF fringe response, which is represented by the term in ω_{LO}, is independent of IF delays; thus the phase of the fringes at a particular point on the sky is constant, whatever IF delay (τ) is used.

From the interferometry geometry,

$$T = \frac{D \sin \Theta}{C}$$

$$= \frac{D}{C} [\sin d \sin \delta + \cos d \cos \delta \cos (H - h)]$$

from equation (1).

Due to the continuous change in H, it is necessary to adjust τ continuously to keep $T = \tau$. However, in this case the term in ϕ_{LO} is independent of τ, so that the fringes remain fixed on the sky. In practice it is found more convenient to track a source by using discrete step changes of τ, small enough to keep $(T - \tau)$ small: this keeps the RF interferometer fringes near to the center of the IF response "envelope".

A rigorous determination of the response of a double passband IF correlation interferometer has been made by Burns [8].

(iii) The relative performance of total power and correlation systems. -- The correlation technique has been considered in some detail by Blum [9], Colvin [10] and other authors. We summarize the differences between the two systems here.

Let the system temperatures be T_1 and T_2, and the source contributions be T_1' and T_2' respectively. If the random gaussian voltages from the two antennas of the interferometer are added, square-law detected and integrated, we have the total power interferometer output

$$\overline{(\sqrt{T_1} + \sqrt{T_1'} + \sqrt{T_2} + \sqrt{T_2'})^2} = \overline{T_1} + \overline{T_1'} + \overline{T_2} + \overline{T_2'} + 2\overline{\sqrt{T_1' T_2'}} \qquad (12)$$

For identical antennas and receivers

$$T_1' = T_2'$$

$$= T'$$

$$= \frac{SA}{2K}$$

where A = effective single antenna area

S = source flux

K = Boltzmann's constant

The only term in equation (12) which contributes to interferometer fringes is the final term, so that

$$\overline{T_A} = 2\overline{T}'$$

$$= \frac{SA}{K}$$

where the averaging (integration) is performed over a time that is short compared with the fringe period.

In the case of the correlation interferometer, we split the voltage from each antenna, and form the sum and difference

$$\left(\sqrt{\frac{T_1}{2}} + \sqrt{\frac{T_1'}{2}} + \sqrt{\frac{T_2}{2}} + \sqrt{\frac{T_2'}{2}}\right) \quad \text{and} \quad \left(\sqrt{\frac{T_1}{2}} + \sqrt{\frac{T_1'}{2}} - \sqrt{\frac{T_2}{2}} - \sqrt{\frac{T_2'}{2}}\right)$$

Each of these quantities is now square-law detected separately, and the difference between the two detected outputs taken. Hence we now have

$$4\left(\sqrt{\frac{T_1}{2}} + \sqrt{\frac{T_1'}{2}}\right) \cdot \left(\sqrt{\frac{T_2}{2}} + \sqrt{\frac{T_2'}{2}}\right)$$

which yields

$$2\sqrt{\overline{T_1 T_2}}$$

as the only non-zero term. As in the total power interferometer, for identical antennas and receivers the correlation interferometer gives

$$\overline{T_A} = \frac{SA}{K}$$

Hence the total power and correlation techniques give the same response to correlated signals, but the latter rejects the uncorrelated terms. In radio astronomy the uncorrelated terms are much larger than the correlated terms, so that receiver instabilities can mask desired signals in the total power interferometer. The correlation interferometer is insensitive to gain fluctuations, except insofar as they change the response to correlated signals. A simple correlator is shown in Figure VI. The NRAO correlator, designed by J. E. Bringe, is shown in Figure VII.

The insensitivity to gain fluctuations can only be achieved if the IF inputs to the correlator are completely isolated and detectors follow a square law over a large dynamic range. The Hewlett-Packard detectors should see a 1000 ohm impedance at their outputs, but due to the inadequate DC gain available after the correlator a much higher output impedance was used, which destroyed the square-law characteristics of the detectors.

For a hybrid with k dB isolation, the correlator output (assuming square law detectors) is now

$$T_A = \left[\left(\sqrt{kT_2} + \sqrt{T_1} + \sqrt{T_1'}\right) + \left(\sqrt{kT_1} + \sqrt{T_2} + \sqrt{T_2'}\right)\right]^2 - \left[\left(\sqrt{kT_2} + \sqrt{T_1} + \sqrt{T_1'}\right) - \left(\sqrt{kT_1} + \sqrt{T_2} + \sqrt{T_2'}\right)\right]^2$$

$$= 4\left(\sqrt{kT_2} + \sqrt{T_1} + \sqrt{T_1'}\right)\left(\sqrt{kT_1} + \sqrt{T_2} + \sqrt{T_2'}\right)$$

We have ignored the terms $\sqrt{kT_1'}$ and $\sqrt{kT_2'}$, since they are very small. When $T_1' = T_2' = T'$ integration gives

$$\overline{T_A} = 4\,\overline{T'} + 8\,\overline{\sqrt{T_1 T_2}}\,\sqrt{k}$$

Hence a 0.2 dB gain change in one arm of the interferometer gives a deflection

$$0.2\sqrt{T_1 T_2}\sqrt{k}$$

For a 200 °K system temperature such a gain change is equivalent to a 0.4 °K signal deflection when the hybrid isolation is 40 dB. A 1 dB gain change would give approximately 2 °K, which is equivalent to the fringe amplitude of 3C 48. At NRAO, automatic gain control is used to control the level of each IF input to the correlator, although such a system will introduce errors (a) if the system noise temperature changes, and (b) when observing strong sources.

For a total power system with noise temperature T, the rms noise fluctuations are given by

$$\Delta T_{TP} = \gamma \frac{T}{\sqrt{\phi \cdot \Delta f}}$$

where γ = a constant whose value lies between 0.71 and 1.0.

Blum [9] and others have shown that for a correlation system

$$AT_{corr} = 0.71\,\gamma \frac{T}{\sqrt{\phi \cdot \Delta f}}$$

For the NRAO interferometer

$$A = 250\ m^2$$

$$T \simeq 200\ °K$$

$$\phi = 0.1\ s$$

$$\Delta f = 10\ MHz$$

Hence for the total power system

$$\frac{T_A}{\Delta T_{TP}} \simeq \frac{0.88 \times 10^{26}}{\gamma} \cdot S$$

and for the correlation system

$$\frac{T_A}{\Delta T_{corr}} \simeq \frac{1.25 \times 10^{26}}{\gamma} \cdot S$$

It should be borne in mind that T_A (fringe amplitude) corresponds to one-half of the peak-to-peak signal on the chart.

Inspection of NRAO interferometer records, for point sources of known flux, indicates that

$$\frac{T_A}{\Delta T_{corr}} \simeq 10^{26} \cdot S$$

Since $\gamma \nmid 1$, other reasons for the low observed signal-to-noise ratio have to be determined. These could be:

(a) Fluctuations in signal level due to imperfect isolation of the two correlator inputs, and to non-square-law detectors,

(b) $T > 200$ °K,

(c) Reduced antenna efficiencies (and hence reduced effective areas),

(d) Lower source fluxes, and

(e) Dispersion in the IF cables.

The combination of reasons (a), (b), (c) and (d) is more than adequate to explain the discrepancy. Reason (e) is worth brief consideration, since it could considerably reduce signal-to-noise ratios for long baseline interferometers with values $\frac{\Delta f}{f_{IF_0}} \simeq 1$ (as at NRAO): this problem is considered in Appendix II, and appears to give negligible effect.

IV. INSTRUMENTAL DESCRIPTION

The interferometer system is shown in Figure VIII. The system in each arm consists of an uncooled parametric amplifier followed by a crystal mixer and intermediate frequency amplifier. The system temperature is approximately 200 °K. The local oscillator frequency corresponds to the center of the parametric amplifier passbands, to give "double passband" operation (Fig. IV). The outputs of each final intermediate frequency amplifier are correlated by means of an analog multiplier followed by an integrator, as described in the previous section. The local oscillator is at 1347.5 MHz, and is locked to a crystal oscillator whose frequency is continuously monitored. The LO is transmitted through buried cables from the central location to a frequency doubler at each antenna. Cables are buried 1.25 meters underground, where temperature variations have been observed to be less than 0.1 °C in 24 hours.

In the previous section it has been shown that, for a symmetrical double passband system, the fringes may only be moved by variations in the differential electrical paths in the local oscillator cables or by variations in the radio frequency paths to the mixers. Hence variations in intermediate frequency paths do not affect phase or position measurements if signal and image responses are identical. The theoretical instrumental equator corresponds with the interferometer response maximum if electrical delays from mixers to the correlating point are equal (i.e., $T = \tau$). Away from instrumental equator the response decreases due to the term

$$\cos \omega_{LO}(T - \tau) \frac{\sin \frac{\Delta\omega(T - \tau)}{2}}{\frac{\Delta\omega(T - \tau)}{2}}$$

. Figure IX shows a compressed record of the interferometer fringes in the region of instrumental equator transit. The slight asymmetry of the record is due to using Cygnus A, which gives the best signal-to-noise ratio but a fringe amplitude (and phase) change due to its structure (see Fig. XI).

Since the bandwidth function and cosinusoidal envelope have slow spatial variations (compared to the fringe rate), "delay tracking" is achieved by switching discrete lengths of cable into or out of the intermediate frequency path, on either side of the

correlator. This results in a very small variation in signal response if small steps are used. At NRAO a unit delay step corresponds to 32 radio frequency wavelengths ($\simeq$ 12 ns), and the switching rate is controlled by a small digital computer, which was designed and built at NRAO and is described in another internal report [11]. The sky coverage with delay tracking is shown in Figure X for a baseline of 1200 m.

The output of the analog multiplier is passed through a 0.1 second time constant for analog recording, and through a voltage-to-frequency converter and gated counter (gate time 0.1 seconds on the shorter interferometer baselines) to a magnetic tape recorder. A "pre-integrator" (time constant = 0.02 sec) prior to the voltage-to-frequency converter limits excessive noise excursions, to prevent the VFC from "saturating."

Since first observations have been made on sources giving clear interferometer fringes, neither the optimum time constant ($= \frac{1}{\omega_{fringes}}$) nor the slowing down of the fringes (by the "lobe rotation" method) has been used. Since all observations will be interspersed with frequent calibrations on the stronger point sources, the need for this additional integration does not appear to arise (even for sourceswhose fringes are invisible on the analog record): integration of digital output is achieved in the digital computer.

V. THE ZERO FRINGE FREQUENCY PLANE

The plane containing the interferometer baseline and the celestial North pole is the fundamental instrumental plane. All sources cross this plane twice, and when they do the fringe rate drops to zero. For a given interferometer the hour angles at which sources cross this instrumental plane are constant and independent of source declination. For an East-West baseline sources cross the instrumental plane at 6 hours East and 6 hours West. For the NRAO interferometer, with a 62° azimuth, $d_E \simeq + 22°$, $d_W \simeq - 22°$ and sources cross the instrumental plane at 7 hours 10 minutes East and 4 hours 50 minutes West. In the spatial frequency plane, the v-axis crossing corresponds to the instrumental plane crossing. Provided that the radio frequency phase

on either side of the instrumental plane crossing is constant, the adjacent fringes may be used to determine the zero fringe frequency point. Furthermore, the phase at the crossover point gives a very good estimate of the longer (day-to-day) variations of phase. Such a zero fringe-rate is shown for sources 3C 147 and Cygnus A in Figure XI.

A fundamental quantity is the baseline factor, B ($= \frac{D}{\lambda} \cos d$). Thus we may write equation (2) in the form

$$\frac{dn}{dt} = -B \cdot \frac{dH}{dt} \cdot \cos \delta \sin (H - h) \qquad (13)$$

The instrumental plane crossing ($\frac{dn}{dt} = 0$) gives h from sources whose positions are accurately known. Initially the NRAO interferometer used 3C 48, 3C 147 and 3C 196, since good positions are available. By the time observations commenced at the second baseline (1500 m), longer delays were available. Thus instrumental crossover was possible at the lower declinations — where lunar occultations have occurred; in particular, 3C 245 has occultation and optical positions in good agreement, and is a further calibration source.

Results of determinations of the baseline factor (B) for a nominal antenna separation of 1200 meters give

$$B_{1200} = \frac{D}{\lambda} \cdot \cos d$$

$$= 10,000 \pm 1 \text{ wavelengths}$$

when the local oscillator frequency is 2695.0 MHz. A preliminary calculation of the baseline factor for a nominal antenna separation of 1500 m is 12493.72 ± 0.02 wavelengths: the local oscillator frequency was 2694.990 MHz. The improvement in accuracy at the longer baseline is due to a more stable local oscillator frequency, and to improved data reduction techniques. The details of this analysis will be reported in the near future.

Since the crossing of the instrumental plane involves the determination of source hour angles to an accuracy < 0.4 sec time, right ascensions may be determined to the same accuracy. Of particular interest is the $\overset{\text{apparent}}{\wedge}$ discrepancy between the optical and radio right ascensions of 3C 286, which supports the observations on the Malvern interferometer (at 610 MHz) [12]: this discrepancy is approximately 1.3 seconds of time, assuming the optical and radio position correspondence for 3C 48. This has yet to be confirmed.

VI. SYSTEM STABILITY AND FIRST OBSERVATIONS

a) System Stability

First observations of fringe phase and amplitude stability were obtained by observing 12 sources as they crossed the instrumental equator. All sources gave fringes with signal-to-rms noise ratios > 10, to permit the time of the peak of each fringe to be determined. Since maximum day-to-day phase shifts were < 90°, it was possible to identify each fringe uniquely and hence to determine short and long term phase drifts. Short term drifts are those which occur over a few minutes, and include the effect of receiver noise. Long term drifts are the random day-to-day variations which occurred over the 10 consecutive days of observations. Figure XII shows the rms phase fluctuation for each source, and appears to indicate a diurnal cycle in the magnitude of the fluctuations. The magnitude of these fluctuations increases throughout the day to reach a maximum in the early evening, which is in agreement with observations of tropospheric radio path fluctuations [13]. However, this correlation should be treated with caution until further results are available.

Average fringe amplitudes during this period were found systematically to decrease by 20 percent in 10 days but this was largely the result of a reduction in the gain of one of the parametric amplifiers. Better amplitude stabilities have since been obtained.

Several experiments have been conducted on the stability of the RF and LO sections, and these have indicated phase variations < 20° in 24 hours.

b) Transit Observations

Table I shows the visibility amplitudes for radio sources observed with the NRAO interferometer. It has been assumed that the visibility amplitude of 3C 147 is unity, so that other fringe visibility amplitudes are given by

$$A = \frac{X}{9} \times \frac{S'}{S}$$

where χ = fringe amplitude (mm on chart),

S' = total flux of 3C 147, and

S = total flux of measured source.

The values of A determined from fluxes measured by Kellerman [14] are designated A_{CIT}. Values of A determined from fluxes measured at NRAO [15] are designated A_{NRAO}.

Using NRAO flux measurements at 2695 MHz, the sources 3C 48, 3C 119, 3C 161, 3C 196, 3C 279, 3C 286, 3C 295, and 3C 345 appear to be unresolved. These results appear to be confirmed by first results of delay tracking. No NRAO flux is available for 3C 245. Source 3C 273 gives a visibility amplitude of 0.86, which is in good agreement with that calculated from the lunar occultation results obtained at NRAO at 11 cm by von Hoerner and Keen (1964). The occultation gives the fluxes $S_B = 30 \pm 5$ W m^{-2} Hz^{-1} and $S_A = 9 \pm 5$ W m^{-2} Hz^{-1}.

Sources 3C 274 and 3C 461 have been observed at equator transit, and with some fixed delays. Both sources give visibility amplitudes which vary with delay, and in particular 3C 461 gives a very interesting result: it is found that when a very long delay is in the eastern arm of the interferometer, the visibility amplitude is too large (by a factor of two) for 3C 461 to be a 4 minute-of-arc disc. A possible explanation could be a fine filament or ridge, which would be in agreement with the large phase change at shorter E-W spacings observed by Moffet [16], and at shorter N-S spacings by Maltby [17].

c) Complete Delay Tracking

In order to illustrate the potentialities of the method, a compressed record of a complete delay track of 3C 405 is shown in Figure XI. This yields information on the brightness distribution along the elliptical arc corresponding to $\delta \simeq 40°$ for a nominal interferometer baseline of 1200 m (Fig. III). Figure XIII shows the positions of visibility amplitude maxima and minima from Rowson at 10.7 cm (R), Lequeux at 21 cm (L) and NRAO at 11 cm (N). Maxima are marked X and minima 0. There is not

yet a track for the nominal baseline of 1500 m. Moffet [18] has indicated that the separation of the two components increases with resolution at 10.6 cm; it is possible to interpret Figure XII in the same way, but apart from the probable existence of a "bridge" between the two main components, too little data is available for further interpretation.

VII. FURTHER DEVELOPMENTS

The installation of a phase lock loop in the local oscillator path [19] and a 70 °K parametric amplifier will considerably improve the interferometer performance. At present, however, too little is known about the phase and amplitude stability of the system (including the atmosphere) and some extensive stability studies will be undertaken in the near future.

A method of correlating the signals entirely by digital methods would be to heterodyne the IF signal from each antenna down to video frequencies, and to pass the video signals through a low-pass filter (frequency range zero to B) prior to clipping. This procedure is similar to that of Weinreb [20]. The two filtered and clipped signals are now sampled at a rate 2B, and corresponding points on each sample multiplied together. This process is then repeated with one or other set of samples delayed. The products for each delay are then added separately over a discrete fraction of a fringe period (for a given number of sample products, n). This gives points on the digital fringe pattern. Thus, the fringe pattern will be digitally reconstituted if the sample products are added over times small compared to the fringe period but large compared to the sampling interval. Since we are now considering digital signals, the problems of amplification and transmission are a standard communications technique. There only remains the problem of synchronizing the two "records". The delay in receiving the digital record from the "distant" antenna presents no problem if there are facilities for storing the digital record from the "home" antenna until the "distant" pulses arrive. One of the difficulties in the use of clipped noise is the retention of fringe amplitudes.

The unclipped amplitudes can only be deduced from the clipped amplitude and a knowledge of the system noise temperature. The method is considered in considerable detail in an internal report [21]. This method is particularly useful for interferometer observations of spectral lines, since the autocorrelation receiver may easily be converted into a cross-correlation receiver.

APPENDIX I

$$R(\tau) = \int_{-\infty}^{\infty} f(t) \cdot (f(t - \tau)\, dt$$

The fourier transformation of $R(\tau)$

$$G(\omega) = \int_{\tau} e^{j\omega\tau}\, d\tau \left[\int_{t} f(t) \cdot f(t - \tau)\, dt\right]$$

$$= \int\int f(t) \cdot f(t - \tau)\, e^{j\omega\tau} dt\, d\tau$$

Let $t = t$ and $T = t - \tau$.

Then $G(\omega) = \int_{t}\int_{T} f(t) \cdot f(T)\, e^{j\omega(t - T)}\, dt\, dT$

$$= \left[\int_{t} f(t)\, e^{j\omega t}\, dt\right] \left[\int_{T} f(T)\, e^{-j\omega T}\, dT\right]$$

$$= F(\omega) \cdot F^*(-\omega)$$

$$= |F(\omega)|^2 \quad \text{if F is real.}$$

Hence $G(\omega)$ is the fourier transform of $R(\tau)$.

APPENDIX II

If a broadband IF signal is transmitted along a dispersive cable, the relative phases of the component sine waves change as the signal passes down the cable. If two such signals pass down equal lengths of cable, correlating the broad-band output signals would result in zero output if the length of the cable were correctly determined for the given dispersion characteristics.

In the NRAO interferometer the IF return cable (from each antenna to the correlating point) has the dispersion characteristics shown in Figure XIV [22]. Since the IF response falls off rapidly below 2 MHz, the maximum differential delay across the IF band is less than 14 ns for 600 meters of cable. This corresponds to a phase lag of approximately 10° at the low frequencies, and a negligible reduction in signal-to-noise ratio. For the longest interferometer baseline (2700 meters) the dispersion in the IF cables to the correlating point gives less than 2 percent deterioration in signal-to-noise ratio. The method of calculating this quantity is as follows:

The IF response is of the form

$$F = \frac{\sin\left(\frac{\omega_2 - \omega_1}{2}\right)\tau}{\left(\frac{\omega_2 - \omega_1}{2}\right)\tau} \cos\left(\frac{\omega_2 + \omega_1}{2}\right)\tau$$

Consider the (rectangular) IF passband to be divided into many small passbands of width b (see Fig. XV). Since we are only interested in the difference in delay across the band, we subtract the shortest delay (at 12 MHz) from all delays determined from Figure XIV. The differential delay for each small passband-center is determined, and all individual narrow-band responses are summed to obtain the total response.

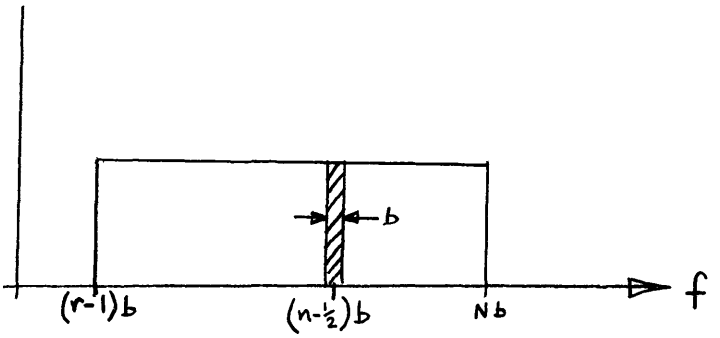

Figure XV

$$\Delta F_n = \frac{\sin\left[2\pi \cdot \frac{b}{2} \cdot \tau_n\right]}{2\pi \cdot \frac{b}{2} \cdot \tau_n} \cos\left[2\pi \; n - \frac{1}{2} \; b \cdot \tau_n\right]$$

$$\text{Total response} = \sum_{n=r}^{n-N} \Delta F_n$$

For b = 0.25 MHz and a rectangular IF passband from 2 to 12 MHz

$$\text{Total response} = \frac{1}{40} \sum_{n=9}^{48} \frac{\sin \frac{\pi}{4} \tau_n}{\frac{\pi}{4} \tau_n} \cos \frac{\pi}{4} (2n - 1) \cdot \tau_n$$

where

$$\tau_n = \frac{4.84 \times 10^{-3}}{n - \frac{1}{2}\; 0.25} - 0.000398.$$

TABLE I

PRELIMINARY FRINGE AMPLITUDES ON THE NRAO INTERFEROMETER
(June-July 1964)
λ = 11.1 cm b = 1200 m

Source Observed	Approx. Fringe Amp (mm)	A_{CIT}	A_{NRAO}	Comments
3C 10	--	--	--	
3C 17	--	--	--	
3C 33	2*	0.38		
3C 48	6	[0.94]	[1.07]	Theoretically $A_{CIT} = A_{NRAO} = 1.0$
3C 71	0.5‡	0.18	0.26	
3C 84	4	0.69	0.84	
3C 111	1‡	0.13	0.16	
3C 119	3.5	1.08	1.12	
3C 123	5	0.27	0.30	
3C 144	<1	--	--	
3C 145	--	--	--	
3C 147	9	1	1	Relative flux standard
3C 161	6	0.74	0.93	
3C 196	5	0.87	1.10	
3C 218	2*	0.14	--	
3C 225	<1	--	--	
3C 231	<1	--	--	
3C 245	2	0.90	--	Occultation model gives A $\simeq$ 1.
3C 273	20	0.77	0.86	Occultation model gives A $\simeq$ 0.85
3C 274	--	--	--	
3C 275.1	<1	--	--	
3C 279	4.5	1.26	1.01	
3C 286	7	0.83	0.99	
3C 287	2.5	0.73	--	
3C 295	7	0.82	0.99	
3C 298	1.5	0.81	--	
3C 305	<1	--	--	
3C 345	5.0	1.13	1.17	
3C 348	1.5	0.08	--	
3C 353	--	--	--	
3C 380	6	0.91	0.90	
3C 405	105	0.16	0.23	
3C 433	--	--	--	
3C 452	--	--	--	
3C 461 Equator	7	0.006	0.008	1 1/2 hours W.
3C 461 Delay	35	0.03	0.04	5 1/2 hours E.
3C 465	--	--	--	
NGC 6946	--	--	--	
NGC 7027	1.5‡	--	0.35⊙	
Jupiter	--	--	--	

⊙ From approximate flux communicated by T.K. Menon. * Denotes noisy records: Fringe amplitude possibly an underestimate. ‡ Analog record reduced. A_{NRAO} represents amplitudes based on relative flux measurements at NRAO at λ = 11.1 cm.

REFERENCES

[1] Keen, N. J., 1964, "Radio Interferometry" (NRAO Lecture Notes).

[2] Read, R. B., 1963, Ap.J., 138, 1.

[3] Rowson, B., 1963, M.N.R.A.S., 125, 177.

[4] Arsac, J., 1961, "Transformation de Fourier et Theorie des Distributions" (Dunod, Paris).

[5] Bracewell, R. N. and Roberts, J. A., 1954, Aust. J. Phys., 7, 615.

[6] Ryle, M. and Hewish, A., 1960, M.N.R.A.S., 120, 220.

[7] Wade, C. M., 1963, private communication.

[8] Burns, W. R., 1964, PhD Thesis (Carnegie Institute of Technology).

[9] Blum, E. J., 1959, Ann. d'Ap., 22, 140 (English translation at NRAO).

[10] Colvin, R. S., 1961, Stanford Radioscience Lab. Report No. 18 (Stanford University).

[11] Keen, N. J., 1964, NRAO Electronics Division Internal Report No. 41.

[12] Hey, J. S., 1964, IAU Meeting, Hamburg.

[13] Thayer, G. D., 1964,

[14] Kellerman, K. I., 1964, A. J., 69, 205.

[15] Keen, N. J., 1964, "Relative and Absolute Flux Measurements of 14 Radio Sources".

[16] Moffet, A. T., 1962, Ap.J. Suppl., 7, 93.

[17] Maltby, P., 1962, Ap.J. Suppl., 7, 124.

[18] Moffet, A. T., 1964, Science, 146, 764.

[19] Bringe, J. E., 1963, NRAO Electronics Division Internal Report No. 21.

[20] Weinreb, S., MIT, Electronics Research Lab., Technical Report No. 412.

[21] Keen, N. J., 1963, NRAO Electronics Division Internal Report No. 19.

[22] Coe, J. C., 1964, private communication.

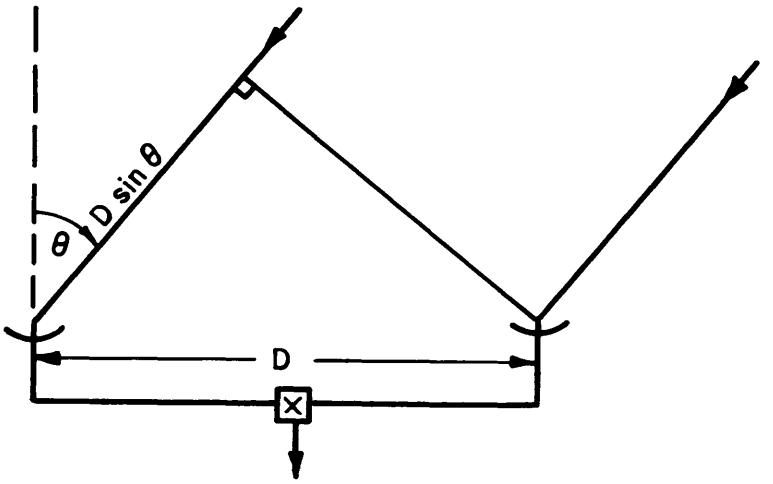
D sin θ
θ
D

Fig. I

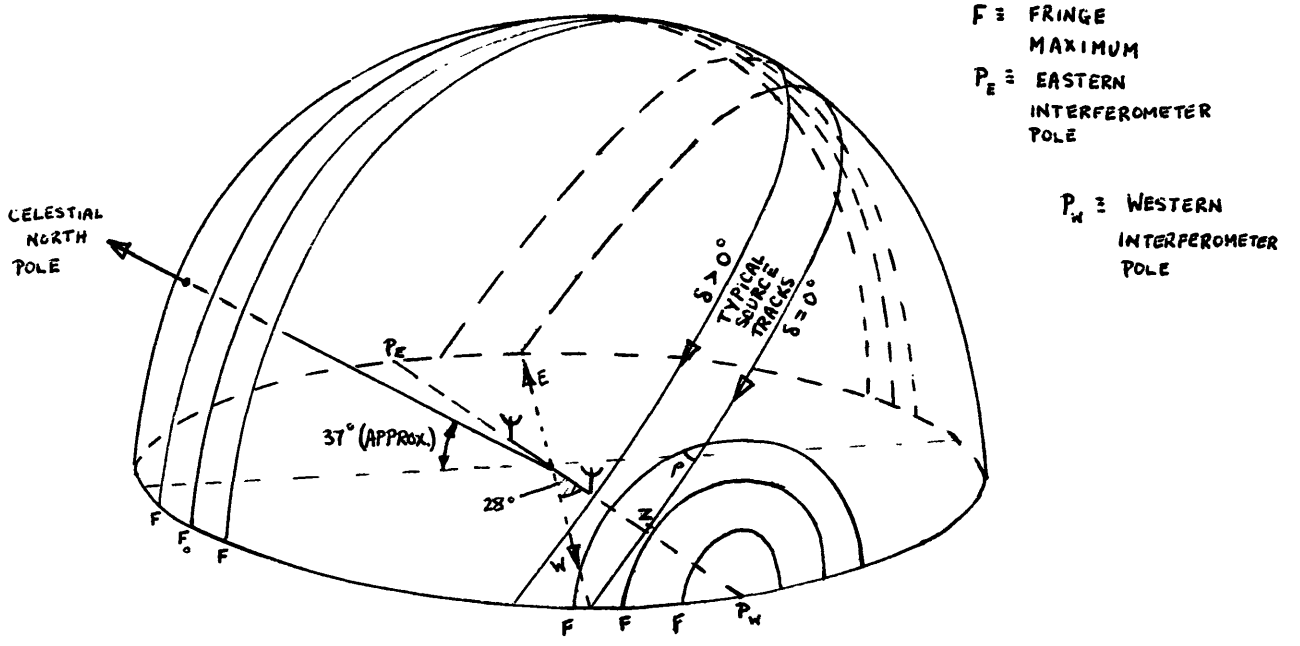
F ≡ FRINGE MAXIMUM
P_E ≡ EASTERN INTERFEROMETER POLE
P_W ≡ WESTERN INTERFEROMETER POLE
CELESTIAL NORTH POLE
δ > 0°
TYPICAL SOURCE TRACKS
δ = 0°
P_E
E
37° (APPROX.)
28°
N
W
F
F
F
F
F
F
P_W

Fig. II

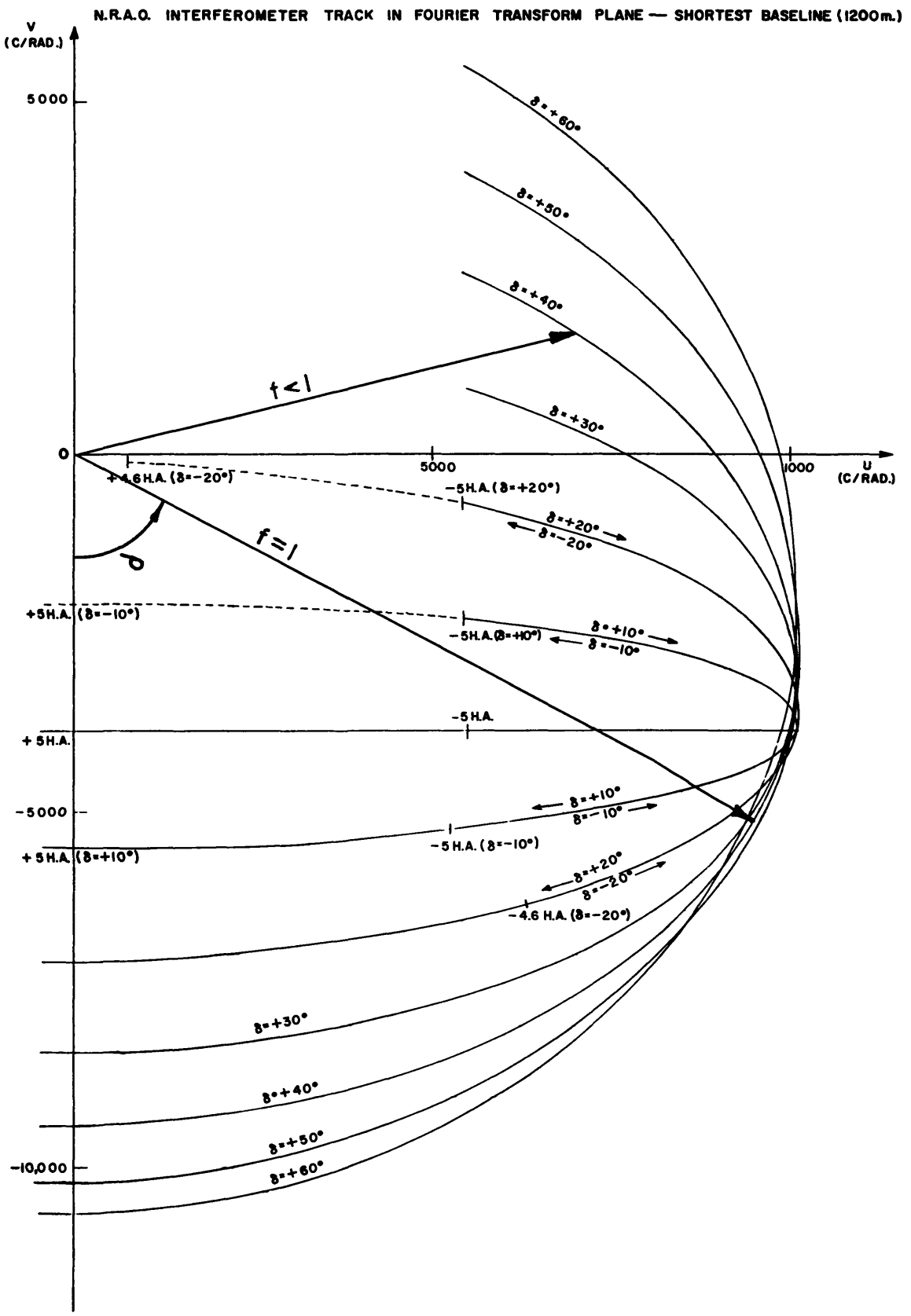
N.R.A.O. INTERFEROMETER TRACK IN FOURIER TRANSFORM PLANE — SHORTEST BASELINE (1200m.)
V (C/RAD.)
5000
0
-5000
-10,000
U (C/RAD.)
5000
1000
t<1
t=1
δ
δ=+60°
δ=+50°
δ=+40°
δ=+30°
δ=+20°
δ=-20°
δ=+10°
δ=-10°
+4.6 H.A. (δ=-20°)
-5 H.A. (δ=+20°)
+5 H.A. (δ=-10°)
-5 H.A. (δ=+10°)
-5 H.A.
+5 H.A.
-5 H.A. (δ=-10°)
+5 H.A. (δ=+10°)
-4.6 H.A. (δ=-20°)

Fig. III

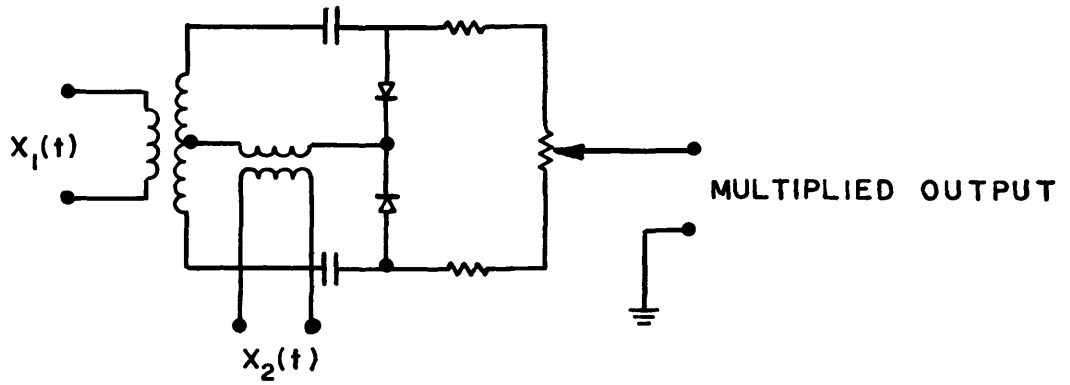

Fig. VI

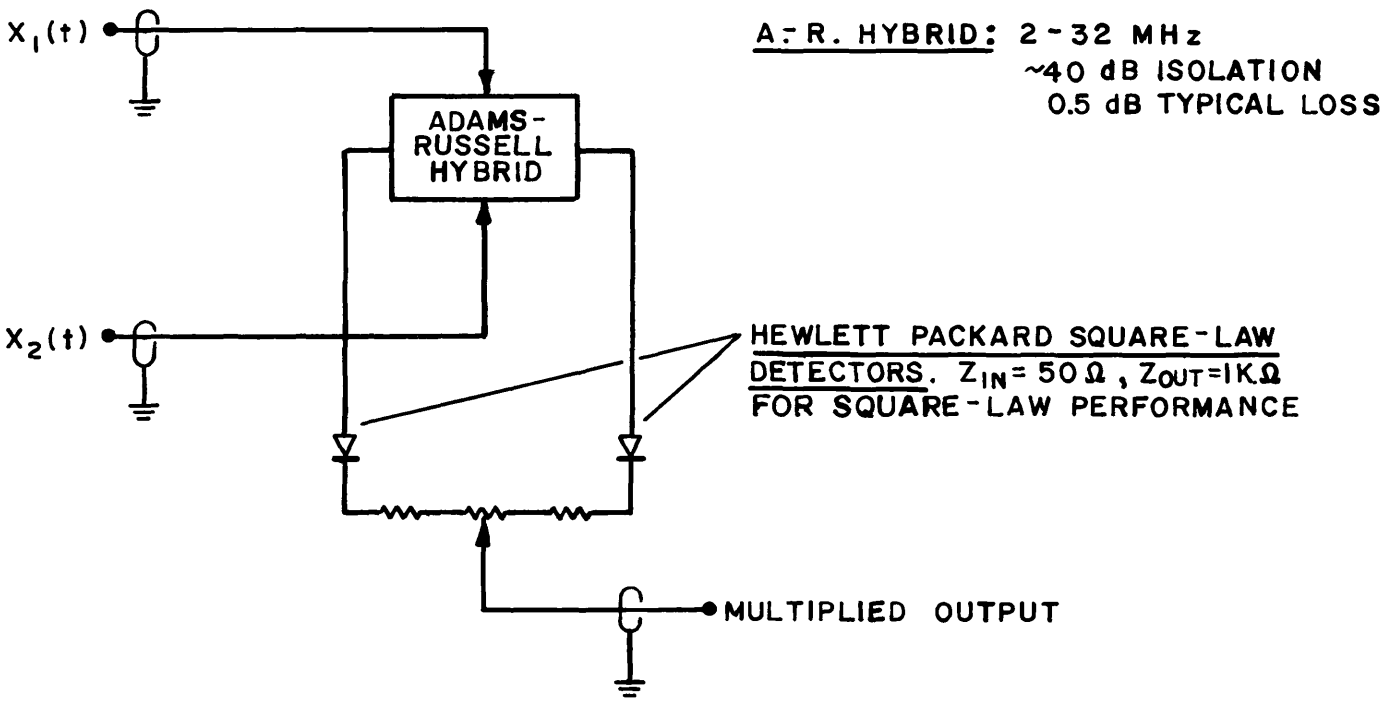

ERRATUM: One of the detectors in Figure VII should be reversed.

Fig. VII

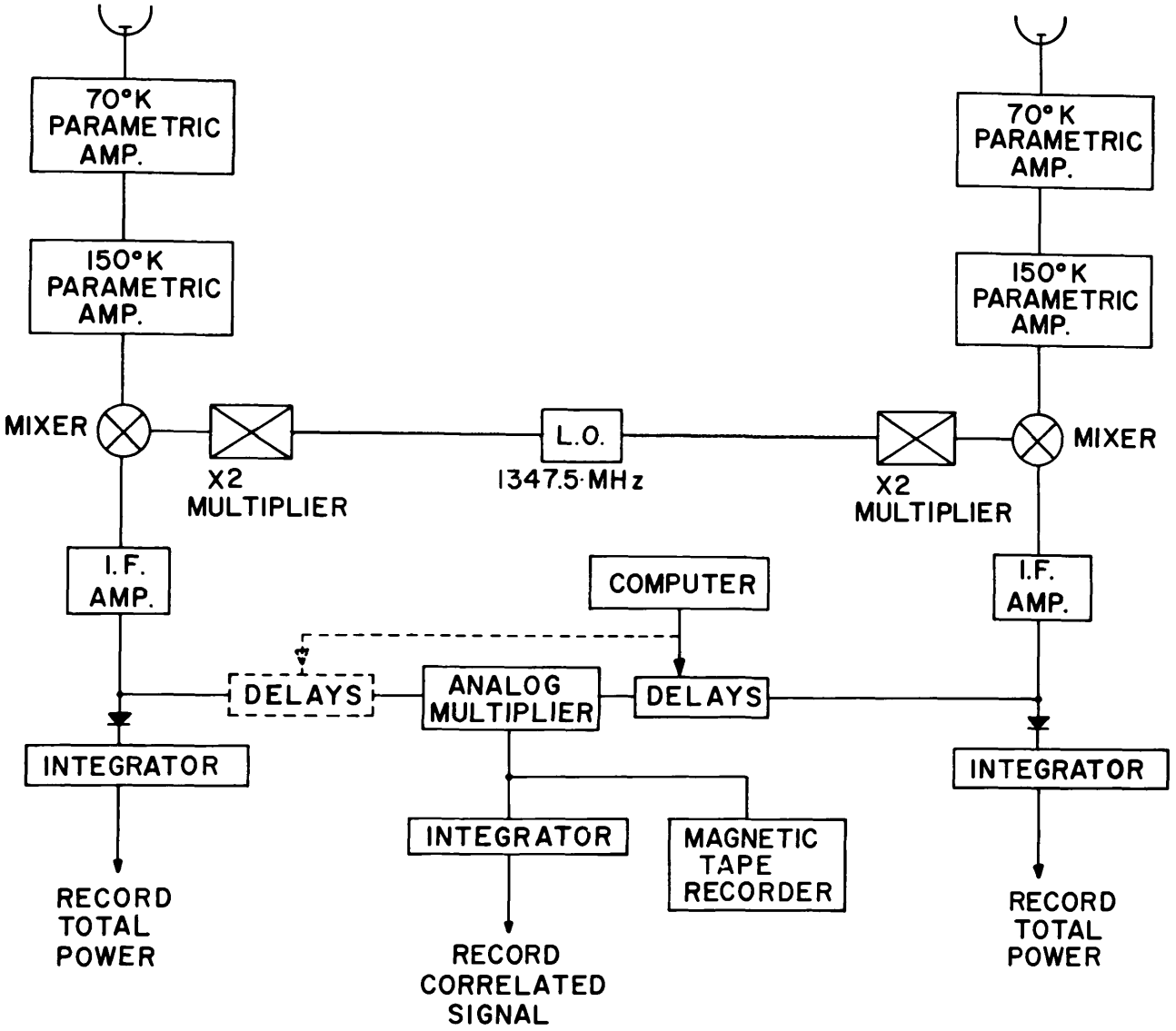
70°K PARAMETRIC AMP.
150°K PARAMETRIC AMP.
MIXER
X2 MULTIPLIER
L.O.
1347.5 MHz
X2 MULTIPLIER
MIXER
70°K PARAMETRIC AMP.
150°K PARAMETRIC AMP.
I.F. AMP.
COMPUTER
I.F. AMP.
DELAYS
ANALOG MULTIPLIER
DELAYS
INTEGRATOR
INTEGRATOR
MAGNETIC TAPE RECORDER
INTEGRATOR
RECORD TOTAL POWER
RECORD CORRELATED SIGNAL
RECORD TOTAL POWER

FIG VIII

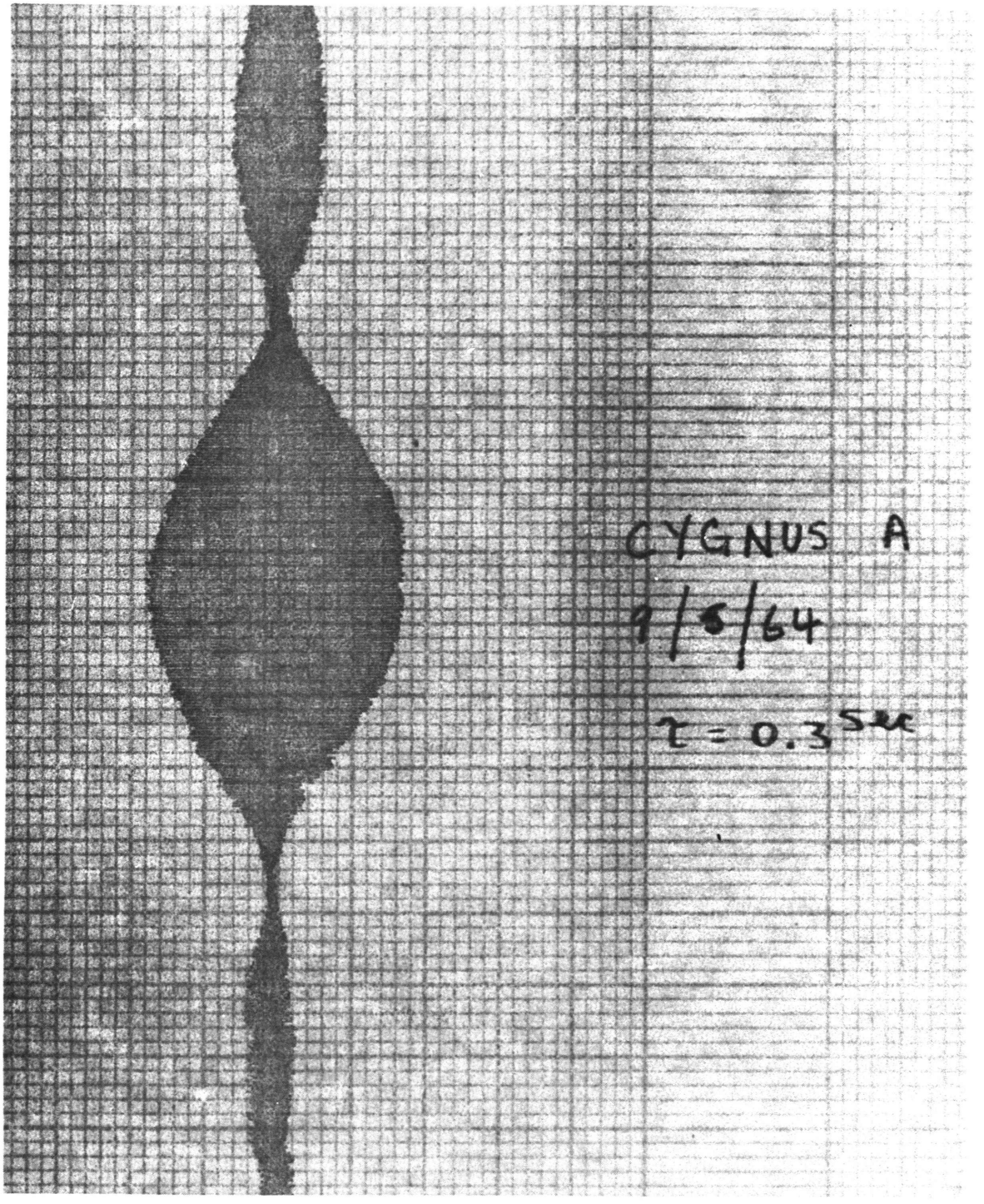

Fig. IX

SKY COVERAGE OF N.R.A.O. INTERFEROMETER WITH DELAY TRACKING-1200m BASELINE

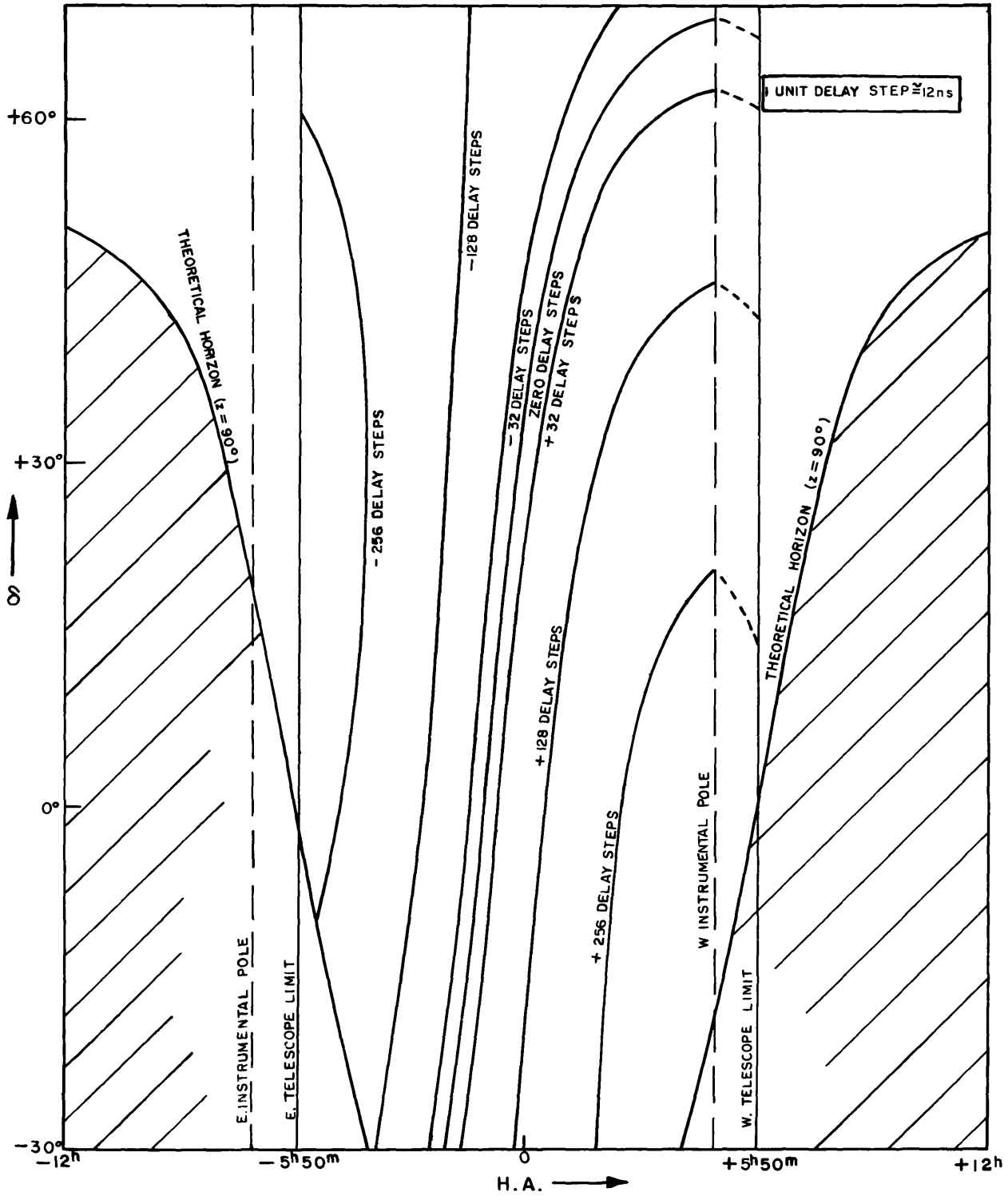

Fig. X

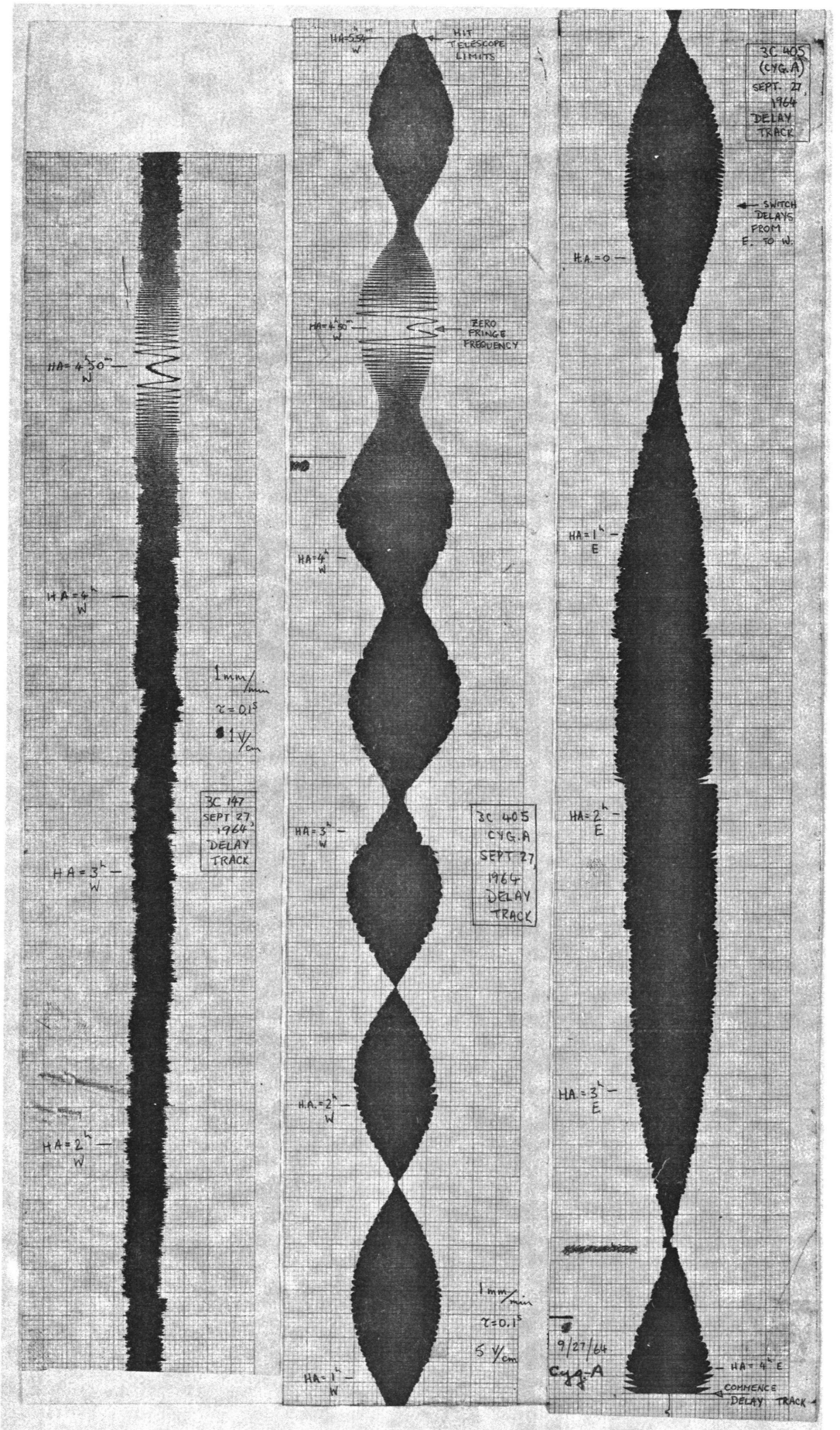
HA = 5h 5m W
HIT TELESCOPE LIMITS
HA = 4h 30m W
ZERO FRINGE FREQUENCY
HA = 4h W
HA = 3h W
HA = 2h W
HA = 1h W
1 mm/min
τ = 0.1s
5 V/cm
3C 405 CYG. A SEPT. 27 1964 DELAY TRACK
HA = 4h 30m W
HA = 4h W
HA = 3h W
HA = 2h W
1 mm/min
τ = 0.1s
1 V/cm
3C 147 SEPT. 27 1964 DELAY TRACK
3C 405 (CYG. A) SEPT. 27 1964 DELAY TRACK
SWITCH DELAYS FROM E. TO W.
HA = 0
HA = 1h E
HA = 2h E
HA = 3h E
HA = 4h E
COMMENCE DELAY TRACK
9/27/64
Cyg-A

Fig. XI

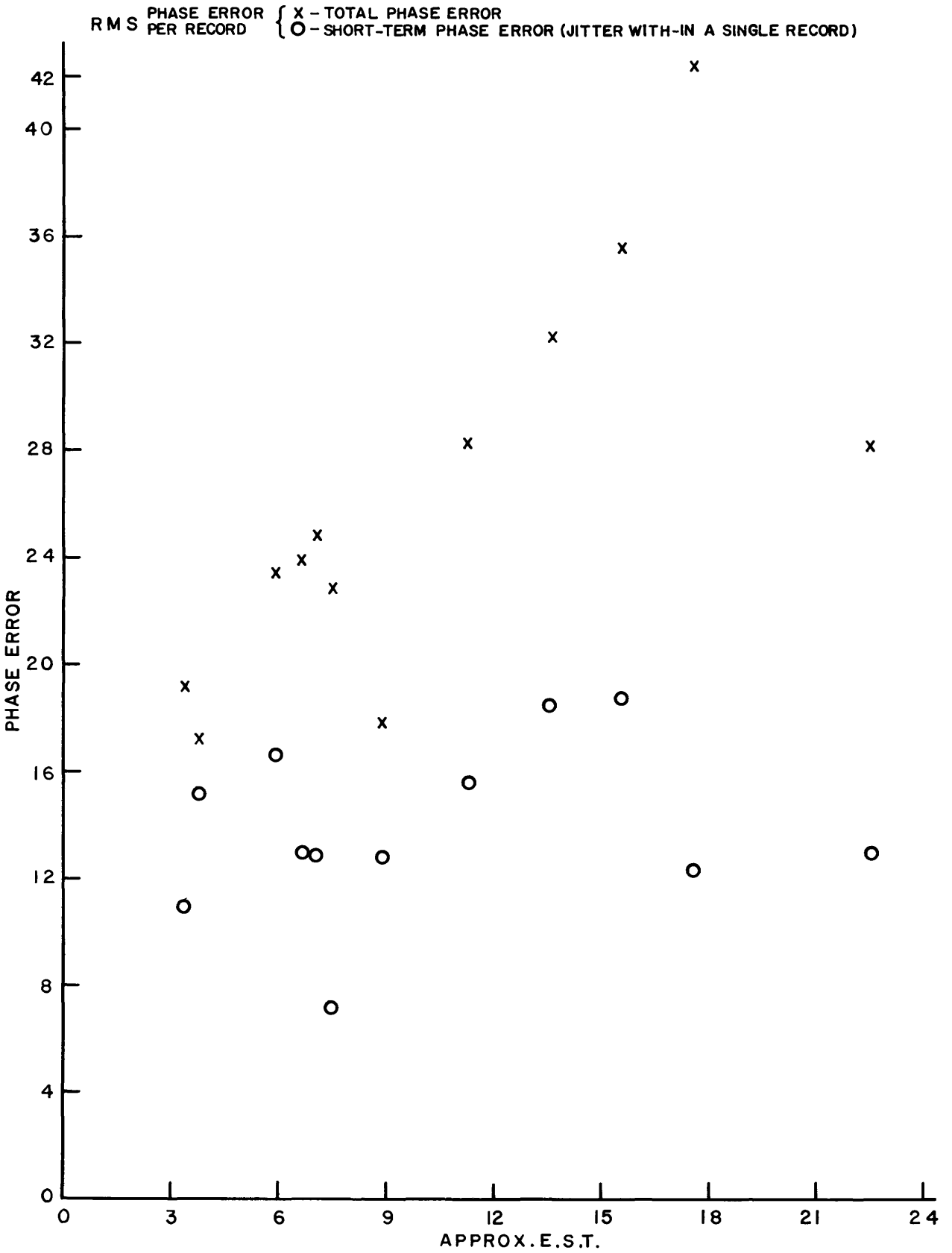
RMS PHASE ERROR PER RECORD
X - TOTAL PHASE ERROR
O - SHORT-TERM PHASE ERROR (JITTER WITH-IN A SINGLE RECORD)
PHASE ERROR
0
4
8
12
16
20
24
28
32
36
40
42
0
3
6
9
12
15
18
21
24
APPROX. E.S.T.

Fig. XII

INTERFEROMETER CONTRIBUTIONS TO THE BRIGHTNESS DISTRIBUTION
OF CYGNUS A

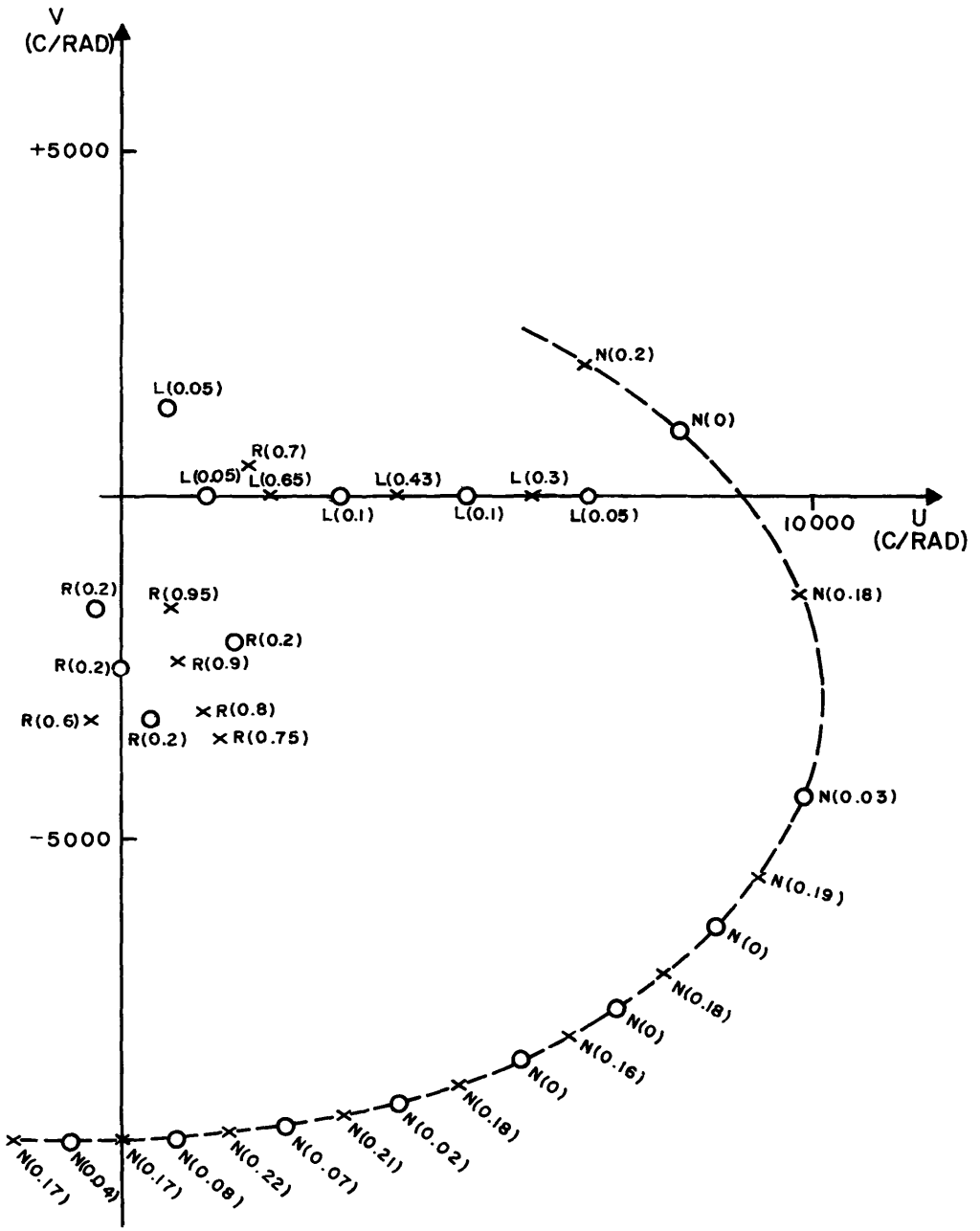

Fig. XIII

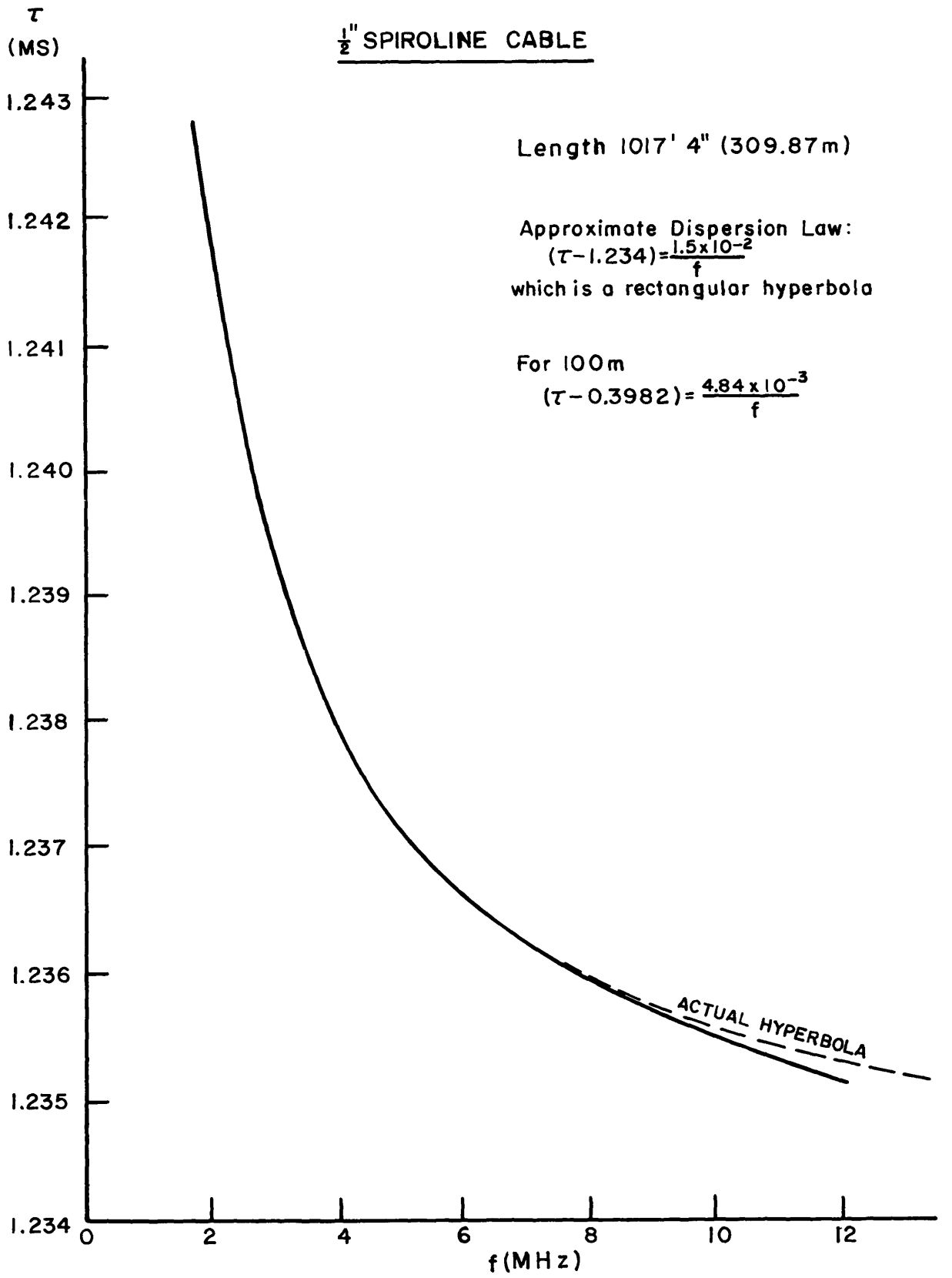
τ
(MS)
½" SPIROLINE CABLE
Length 1017' 4" (309.87m)
Approximate Dispersion Law:
$(\tau - 1.234) = \frac{1.5 \times 10^{-2}}{f}$
which is a rectangular hyperbola
For 100m
$(\tau - 0.3982) = \frac{4.84 \times 10^{-3}}{f}$
1.243
1.242
1.241
1.240
1.239
1.238
1.237
1.236
1.235
1.234
0
2
4
6
8
10
12
f(MHz)
ACTUAL HYPERBOLA

Fig. XIV